Physica E: Low-dimensional Systems and Nanostructures 104 (2018) 64–70

Contents lists available at ScienceDirect

Physica E: Low-dimensional Systems and Nanostructures

journal homepage: www.elsevier.com/locate/physe

Surface optical phonon – Plasmon interaction in nanodimensional CdTe thin films

J. Mitric[a,*], N. Paunovic[a], M. Mitric[b], B. Vasic[a], U. Ralevic[a], J. Trajic[a], M. Romcevic[a], W.D. Dobrowolski[c], I.S. Yahia[d,e], N. Romcevic[a]

[a] Institute of Physics, University of Belgrade, Pregrevica 118, 11080 Belgrade, Serbia
[b] Institute Vinca, University of Belgrade, P.O. Box 522, 11001 Belgrade, Serbia
[c] Institute of Physics, Polish Academy of Science, al. Lotnikov 32/46, 02-668 Warsaw, Poland
[d] Department of Physics, Faculty of Science, King Khalid University, P.O. Box 9004, Abha, Saudi Arabia
[e] Nano-Science & Semiconductor Labs, Department of Physics, Faculty of Education, Ain Shams University, Roxy, Cairo, Egypt

ARTICLE INFO

Keywords:
Thin film
Surface optical phonon
Raman spectroscopy
Far–infrared spectroscopy
Plasmon-phonon interaction

ABSTRACT

Structural and optical properties of CdTe thin films were investigated applying atomic force microscopy (AFM), XRD powder technique, Raman spectroscopy and far–infrared spectroscopy. CdTe thin films were prepared by using thermal evaporation technique. In the analysis of the far – infrared reflection spectra, numerical model for calculating the reflectivity coefficient for system which includes films and substrate has been applied. Effective permittivity of film mixture (CdTe and air) was modeled by Maxwell – Garnet approximation. We reveal the existence of surface optical phonon (SOP) mode and coupled plasmon-SOP modes (CPSOPM).

1. Introduction

II – VI semiconductor compounds, especially thin films, have become very popular because of their applications in numerous electronic and optoelectronic devices. Due to low production cost, thin films nowadays enjoy great attention in basic research and solid state technology.

The interest in various properties of photonic CdTe is well justified, as this material plays an important role in expanding variety of applications as in: integrated optics, optoelectronics, or solar energy conversion [1].

Two main properties of CdTe thin film are its high optical absorption coefficient (a thin film of CdTe with thickness of approximately 2 μm will absorb nearly 100% of the incident solar radiation) and its near ideal band gap for photovoltaic conversion efficiency of 1.45eV [2]. Also, its ease of film fabrication and low cost make it a representative material among II – VI semiconductors.

For fabrication of the CdTe films, various techniques have been applied: RF magnetron sputtering [3], molecular beam epitaxy (MBE) [4], pulsed laser deposition (PLD) [5], successive ionic layer adsorption and reaction method (SILAR) [6], metal organic chemical vapor deposition [7], screen printing [8], thermal evaporation method [9] etc. Thermal evaporation method shows some advantages such as: minimalization of impurities proportional to the growing layer, reduced chances of oxidation and direction of propagation (occurs from the source to the substrate) [9,10]. This makes thermal evaporation technique the most suitable method, thanks to very high deposition rate, low material consumption and low cost of fabrication [11].

In the case of crystal with relatively small dimension, in the frequency range between bulk longitudinal optical phonon frequency (ω_{LO}) and transversal optical phonon frequency (ω_{TO}), a new mode known as a surface phonon mode appears [12,13]. It is known for the case of real crystal, that when its dimension is relatively small, surface modes and effects of dimension will be manifested in addition to the normal modes of infinite lattice. But, when crystal is reduced to extremely small dimensions, only the surface mode will persevere [12–14].

On the other side, electron – phonon interaction takes an important place in semiconducting materials [15]. In our earlier work we have registered plasmon (collective electron excitation) and LO phonons interaction in different systems [16–19]. Besides that, we have studied the impact of damping on interaction appearance [20], interaction between plasmon and different phonons [21,22], as well as interaction between plasmon and impurity local phonons [23–25].

In this work we report experimental studies of CdTe thin films prepared by thermal evaporation technique. Existence of nanodimensional structures in these thin films enabled us to observe effects associated with interactions between surface optical phonon (SOP) and

* Corresponding author.
E-mail address: jmitric@ipb.ac.rs (J. Mitric).

https://doi.org/10.1016/j.physe.2018.07.021
Received 27 April 2018; Received in revised form 5 July 2018; Accepted 16 July 2018
Available online 18 July 2018
1386-9477/

plasmon for the first time.

Samples characterization was performed using atomic force microscopy (AFM). Structural properties were analyzed using XRD powder technique, and optical properties were characterized using Raman and far–infrared spectroscopy.

2. Sample preparation and characterization methods

CdTe single crystal was grown by the Bridgman technique. Different thickness of CdTe thin films were deposited by thermal evaporation from a resistance heating quartz glass crucible onto glass substrates using high vacuum coating unit type Edward 306 A. Films were grown at a pressure of 106 Pa. The mechanical rotation of the substrate holder during deposition produced homogeneous film. The distance between the source heater and substrates holder is 21 cm, in order to avoid any heat flow from the source to the substrates.

The morphology of the four CdTe thin films of different thicknesses was investigated by Atomic force microscopy (AFM). Atomic force microscopy measurements were performed using NT-MDT system NTEGRA Prima. Imaging was done in tapping mode using NSG01 probes. All AFM measurements were done at ambient conditions. For the sake of statistical analysis of sample surface, we calculated histograms and bearing ratios for each topographic image. The histogram represents a height distribution density of all points in a two-dimensional topographic image, or in other words, it is a number of points with height given on x-axis. On the other hand, the bearing ratio curve gives a percent of points in a corresponding two-dimensional topographic image with a height less than the number given on x-axis.

The structural characteristics were obtained by the XRD powder technique. All samples were examined under the same conditions, using a Philips PW 1050 diffractometer equipped with a PW 1730 generator, 40 kV × 20 mA, using Ni filtered Co Kα radiation of 0.1778897 nm at room temperature. Measurements were carried out in the 2 h range of 10–100° with a scanning step of 0.05° and 10 s scanning time per step. Crystallite size was determined by using XFIT computing program which is based on Fundamental Parameter convolution approach [26].

Raman measurements were performed using commercial NTegra Spectra system from NT-MDT. A linearly polarized semiconductor laser operating at a wavelength of 532 nm was used. All the spectra were obtained by setting the laser power to 2 mW within the ~0.5 × 0.5 μm sized focus with exposure time of 600 s.

The far-infrared (FIR) reflectivity measurements were performed at room temperature with a BOMEM DA-8 Fourier-transform infrared spectrometer. A Hyper beamsplitter and deuterated triglycine sulfate (DTGS) pyroelectric detector were used to cover the wave number region from 80 to 650 cm^{-1}.

3. Results and discussion

3.1. Atomic force microscopy

Three dimensional topographic images of all four samples are shown in the left side of Fig. 1. As can be seen, sample surfaces are rather flat, but still they are characterized with bright protrusions and dark holes (which represent air) resulting in a small surface roughness of several nanometers.

In order to characterize fraction of both observed topographic features, the statistical analysis have been performed by calculating histograms and bearing ratios from two dimensional topographic images. The results for all four samples are given in the right side of Fig. 1. They show that the peaks in the histograms are positioned in the middle of bearing ratio curves. Therefore, from these curves we can conclude that the fraction of holes and protrusions are rather similar, around 50%.

In order to estimate thicknesses of studied films, their step edges were measured by AFM. 3D AFM topographic images of the step edges are depicted in Fig. 2(a1-d1). The films are brighter and the substrates are dark in the images, while the step edges are clearly resolved. Based on the AFM images, height distributions were calculated and presented in Fig. 2 (a2-d2). In all histograms, there are two characteristic peaks: a lower one corresponds to the substrate, while a higher one corresponds to the film. Therefore, the film height can be then approximately calculated as a difference between these two peaks. Estimated film thicknesses are given in Fig. 2 (a2-d2). The best resolved height peaks were found on CdTe 1 in Fig. 2 (a2) due to a smooth sample surface as can be seen in Fig. 2 (a1).

3.2. XRD

Structures of four synthesized CdTe thin films with different thicknesses were identified by XRD pattern as shown in Fig. 3. The diffractograms confirm that all samples are monophased, and that they crystallized in sphalerite type structure in 216. space group, $F\bar{4}3m$. All of the observed diffraction peaks are indexed according to this space group. Therefore, in our thin film samples there is no other structures other than CdTe. In this structural type, Cd ions occupy *4a* Wyckoff positions, [[0, 0, 0]] with local symmetry $\bar{4}3m$, while Te ions occupy *4c* Wyckoff positions [[1/4, 1/4, 1/4]] with the same local symmetry. Cd ions are in tetrahedral surrounding of Te ions (and vice versa). The tetrahedrons are regular and share common vertices. Crystallite size (R) is determined and presented in Fig. 2 and Table 1.

3.3. Raman spectroscopy

The cubic face-centered structure of balk crystal CdTe is characterized by the 216. space group $F\bar{4}3m$ and contains four formula units, while the primitive cell is one fourth as many. Optical modes consist of one three fold –degenerated mode F_2 which is active in IR and Raman spectra. The dipole mode F_2 is split into the transverse (TO) and longitudinal (LO) modes in the vibrational spectra. It is very well known that reduction of the particle dimensions to nanoscale results in a breakdown of phonon selection rules and allows phonons with $l \neq 0$ to contribute to Raman scattering [27–31]. Consequently, some new forbidden vibration modes (low frequency region, acoustic modes, and high frequency region, surface optical modes) occur due to imperfections, impurity, valence band mixing and/or nonspherical geometry of the nanostructures [14].

TO (142 cm^{-1}) and LO (170.5 cm^{-1}) modes for the CdTe bulk crystal are both active in the Raman spectra. Also, the modes in band near 120 cm^{-1} correspond to phonons of Te on the CdTe surface and can be seen in the Raman spectra [32].

Raman spectra of CdTe thin films of different thickness at room temperature are presented in Fig. 4.

For analyzing obtained spectra Lorentz profiles were used. Solid lines are their sums. In the top right corner Raman spectra of bulk CdTe crystal for ambient conditions is presented [32]. The observed Raman spectra for all samples among characteristic CdTe TO mode at 142 cm^{-1} and phonon of Te of the CdTe surface (127 cm^{-1}), show the LO phonon like frequency shift from 170.5 cm^{-1} to 164 cm^{-1}. That can be attributed to the surface optical phonon (SOP) mode effect [33–38]. It is clear that SOP phonon is wider compared to LO phonon of bulk crystal, as well as when it's compared to phonon of nanodimensional film. This effect is associated with interaction between SOP and plasmon, which will be mentioned later on.

In order to analyze the surface optical phonon we have to take into account that a part of crystallites are surrounded by air. We will analyze the dependence of the SOP mode position on filling factor (*f*) of the mixed material.

Surface phonon modes can be detected in systems where particle size is much smaller when compared to wavelength of exciting light source [39]. These modes can be obtained for in the case of polar crystals [40], so we consider expression for dielectric function which describes optical properties of polar semi – insulating semiconductor in

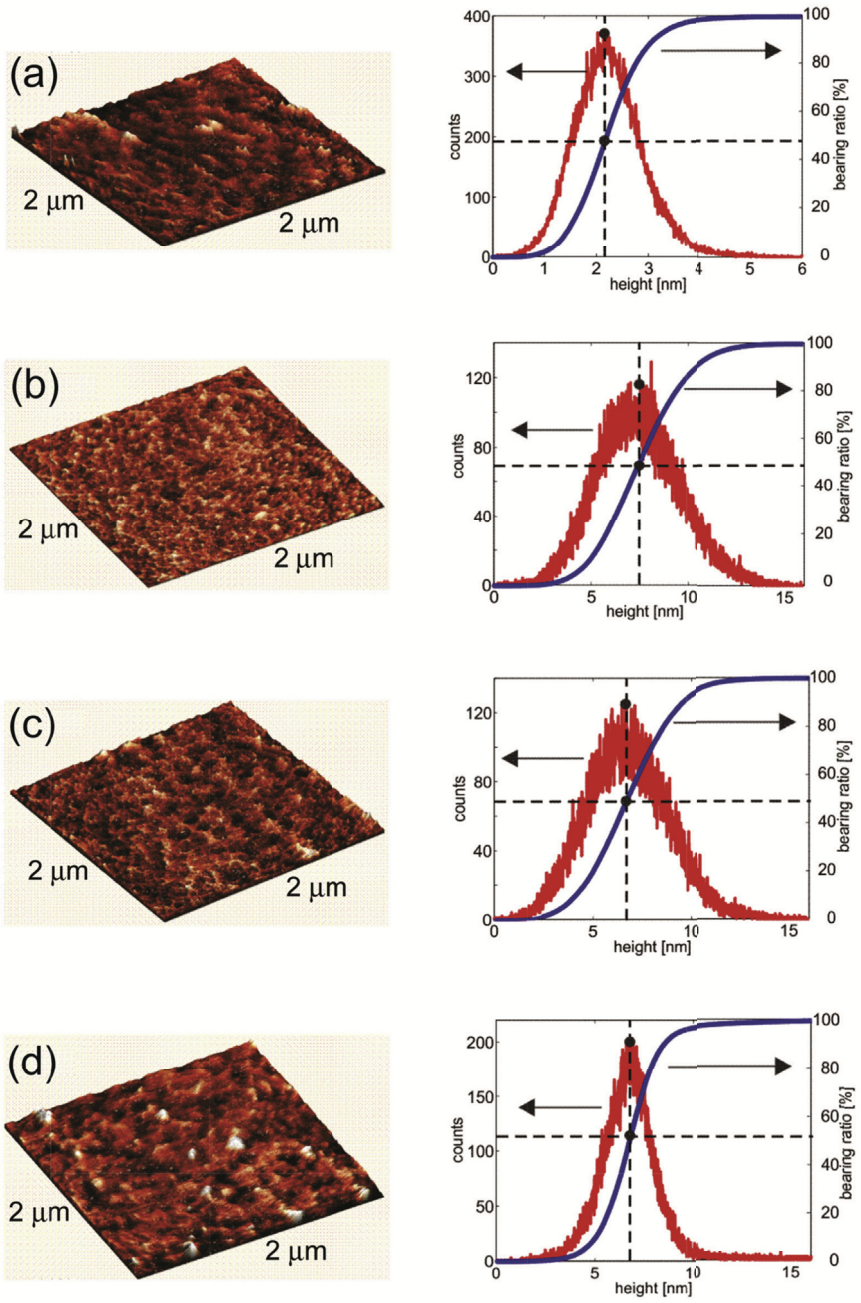

Fig. 1. Three-dimensional topographic image (left) and corresponding histogram and bearing ratio (right) for (a) CdTe 1, (b) CdTe 2, (c) CdTe 3, and (d) CdTe 4. Scan size is 2 μm.

IR region [24]:

$$\varepsilon_2(\omega) = \varepsilon_\infty\left(1 + \sum_{k=1}^{n} \frac{\omega_{LOk}^2 - \omega_{TOk}^2}{\omega_{TOk}^2 - \omega^2 - i\gamma_{TOk}\omega} - \frac{\omega_P^2}{\omega(\omega + i\Gamma)}\right) \quad (1)$$

ωTO and ωLO represent transverse and longitudinal optical bulk phonons, respectively; ε∞ is the dielectric constant at high frequencies, ωP is plasma frequency and γ and Γ are the damping constants. Surface phonons can be considered similarly to phonons in infinite crystals, but with adapted wave functions to the geometry of the small particle.

Here, we will apply effective medium theory: Because the size of semiconducting nanoparticles, L, (with dielectric function ε_2, and are distributed in a medium with dielectric constant ε_1) is considerably smaller than the interacting wavelength of visible light, λ (λ ≫ *L*), we treat the heterogeneous composite as a homogeneous medium.

Even though there are numerous models for the effective dielectric permittivity for these kinds of mixtures [41], we decided to use Maxwell – Garnet model, because all our samples are thin films with well defined and separated nanosized grains. According to the Maxwell – Garnet mixing rule [42,43], effective permittivity of mixture, including spherical geometry of particles is given with:

$$\varepsilon_{eff} = \varepsilon_1 + 3f\varepsilon_1\frac{\varepsilon_2 - \varepsilon_1}{\varepsilon_2 + 2\varepsilon_1 - f(\varepsilon_1 - \varepsilon_2)} \quad (2)$$

In this case, nanoparticles are spheres with permittivity ε_2 and are randomly distributed in homogeneous environment, with permittivity

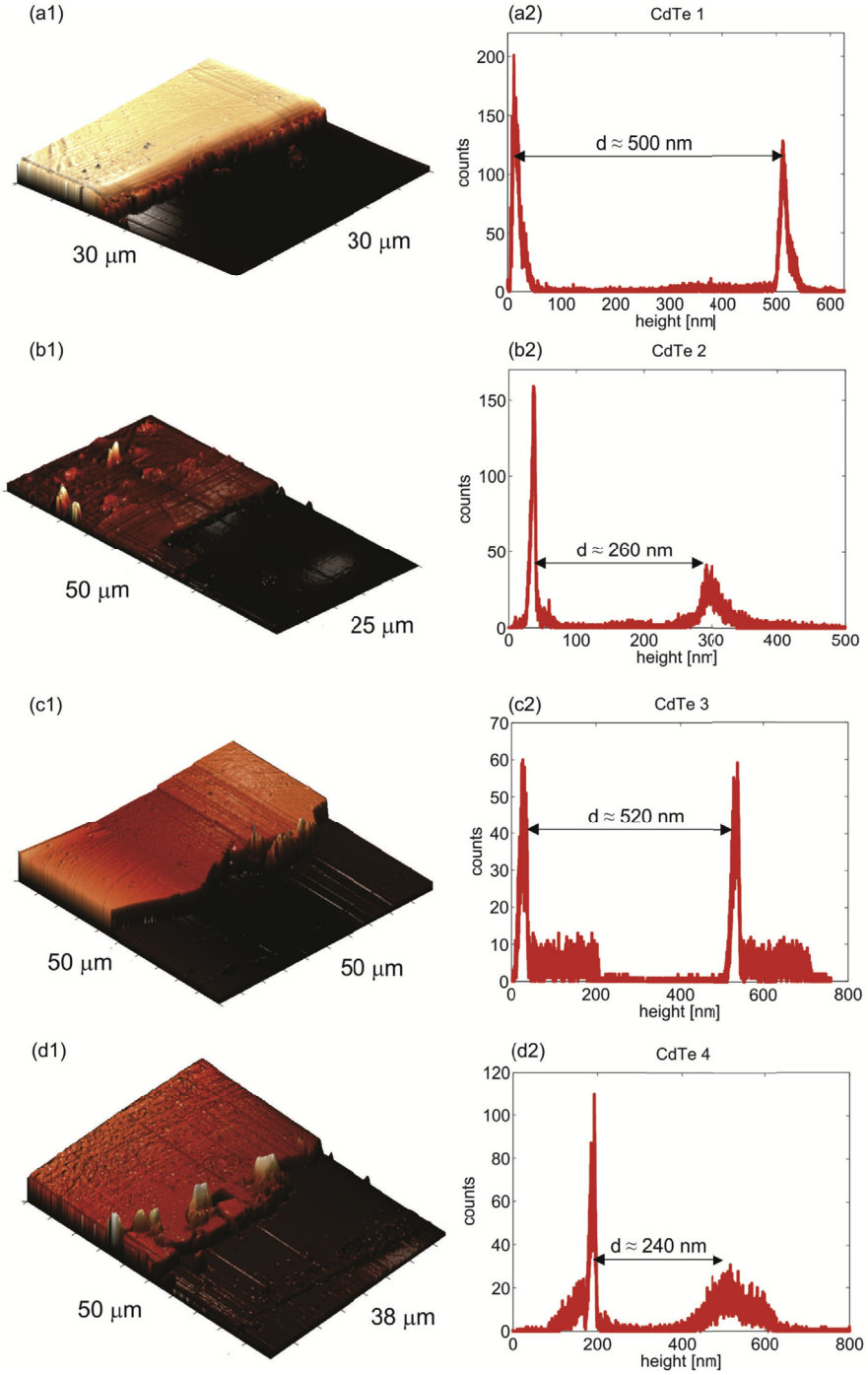

Fig. 2. (a1-d1) 3D AFM topographic images of step edges of studied films, and (a2-d2) corresponding height histograms. Average films thicknesses are denoted in the histograms.

ε_1 and occupy a volume fraction f.

Position surface optical phonon (SOP) mode frequencies are obtained from Ref. [44]:

$$\omega_{SOP} = max\left(I_m\left(-\frac{1}{\varepsilon_{eff}}\right)\right) \tag{3}$$

The result is shown in Fig. 5. The practical liner dependence of the position of the SOP mode on the filing factor f has been obtained. For the frequency of the SOP mode determined in Fig. 4 we have $f = 0.53$. This result is in accordance with the one obtained from the AFM measurements.

3.4. Far-infrared spectroscopy

Thicknesses of our films, as we will see, are in a range from ~0.39 μm to ~0.72 μm, so reflectivity spectra contain information about CdTe films together with information about substrate. Representative scheme of our layered structure can be presented in Fig. 6 [45]. Medium 1 is air, medium 2 is thin bulk CdTe crystal layer and medium 3 is substrate glass, with dielectric functions ε_1 ($\varepsilon_1 = 1$), ε_2 and ε_3, respectively. We can now write [46]:

$$R_A = \frac{A_r}{A_i} = \frac{r_{12}e^{-i\alpha} + r_{23}e^{i\alpha}}{e^{-i\alpha} + r_{12}r_{23}e^{i\alpha}} \tag{4}$$

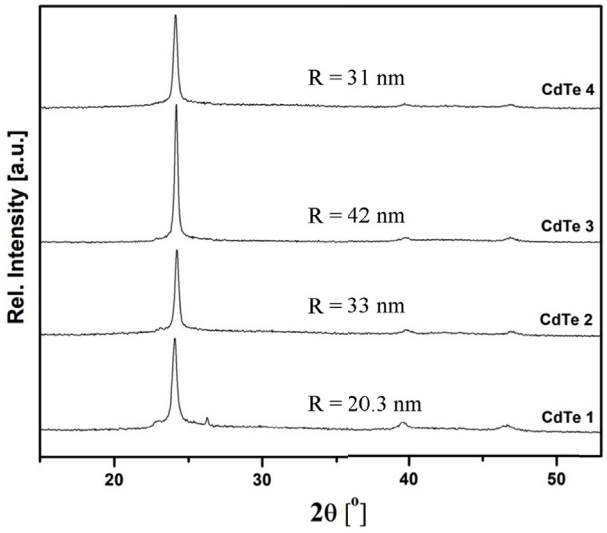

Fig. 3. XRD analysis of CdTe thin films of different thickness. Obtained crystallite sizes (R) are presented too.

Table 1
Parameters obtained from XRD measurements and FIR reflection spectroscopy. Thin films thickness - d, Crystallite size – R.

Name	d [μm]	R [nm]	ω_{l1} (ω_+) [cm^{-1}]	ω_{l2} (ω_-) [cm^{-1}]	ω_P [cm^{-1}]	ω_t [cm^{-1}]	f
CdTe 4	0.39	31.0	187	103	137.5	140.0	0.53
CdTe 2	0.43	33.0	174	78	96.6	140.5	0.53
CdTe 3	0.71	42.0	170	65	79.5	139	0.53
CdTe 1	0.72	20.3	165	30	35.2	140.5	0.53

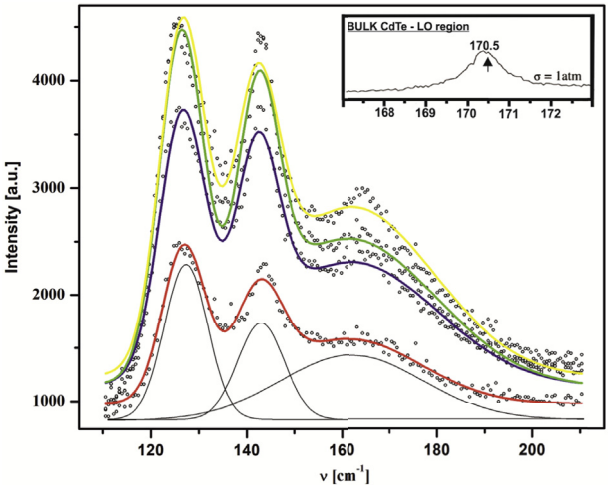

Fig. 4. Raman spectra of CdTe thin films of different thickness. Experimental spectra are shown by open dots. Solid lines are sums of three Lorentz profiles as it shown for spectrum of CdTe 1. In the top right corner LO region of bulk CdTe is presented, taken from the literature [32].

$r_{ij} = (n_i - n_j)/(n_i + n_j) = (\sqrt{\varepsilon_i} - \sqrt{\varepsilon_j})(\sqrt{\varepsilon_i} + \sqrt{\varepsilon_j})$ describe Fresnel coefficients, A_i and A_r represent amplitudes of incident and reflection beams, n is complex index of refraction, ε is the dielectric constant and $\alpha = 2\pi\omega d(\varepsilon_2)^{1/2}$ is the complex phase change related to the absorption in the crystal layer with the thickness d.

Reflectance, R, is given with:

$$R = |R_A|^2 \tag{5}$$

In this case we decided to use dielectric function which takes into consideration the existence of plasmon – phonon interaction in advance.

The dielectric function of the CdTe crystal layer is:

$$\varepsilon_2(\omega) = \varepsilon_{\infty CdTe} \prod_{j=1}^{2} \frac{\omega^2 + i\gamma_{lj}\omega - \omega_{lj}^2}{\omega(\omega + i\Gamma_p)(\omega^2 + i\gamma_t\omega - \omega_t^2)} \tag{6}$$

The ω_{lj} and γ_{lj} ($j = 1, 2$), parameters of the first numerator are the eigenfrequencies and damping coefficients of the longitudinal plasmon-phonon (LP + LO) waves, that arise as a result of the interaction of the initial phonon ($\omega_{LO,CdTe} = 170.5\ cm^{-1}$) and plasmons ($\omega_P$) modes. The parameters of the denominator correspond to the similar characteristics of the transverse vibrations (ω_t, γ_t) and plasmon damping Γ_P. As a result of the best fit, we obtain coupled mode frequencies (ω_{l1} and ω_{l2}).

The dielectric function of the glass substrate is:

$$\varepsilon_s(\omega) = \varepsilon_{\infty\ sup} \prod_{k=1}^{n} \frac{\omega_{LOk}^2 - \omega^2 + i\gamma_{LOk}\omega}{\omega_{TOk}^2 - \omega^2 + i\gamma_{TOk}\omega} \tag{7}$$

where ω_{TO} and ω_{LO} are the transversal and longitudinal optical vibrations, and γ_{TO} and γ_{LO} are damping parameters, respectively.

In our case, layer 2 consists of a CdTe crystals and air (see Fig. 6). The size of the crystallites (R) is given in Fig. 2 and Table 1. These crystallites are described by a dielectric function given in Eq. (1) or Eq. (6) and located randomly in homogeneous environment ε_1 (air) and occupy a volume fraction f, so we can use effective medium theory and Maxwell - Garnet mixing rule, given with Eq. (2).

The far – infrared reflectivity spectrum of the glass substrate is shown in Fig. 7(e). The calculated spectrum, presented by solid line, was obtained using the dielectric function given by equation (7). As a result of the best fit we obtained three modes, whose characteristic frequency are $\omega_{TO1} = 60\ cm^{-1}$, $\omega_{LO1} = 140\ cm^{-1}$, $\omega_{TO2} = 441\ cm^{-1}$, $\omega_{LO1} = 443\ cm^{-1}$ and $\omega_{TO3} = 471\ cm^{-1}$, $\omega_{LO3} = 522\ cm^{-1}$. Frequency values of these modes have remained the same during the fitting procedure for all CdTe thin film samples.

The parameters obtained by the best fit between the experimental results and the models for CdTe film described earlier are also given in Table 1. The far-infrared spectra of CdTe thin films, in the spectral range of 80–600 cm^{-1}, at room temperature, are presented in Fig. 7. Experimental data are presented by circles, while the solid lines are calculated spectra obtained by a fitting procedure based on the previously presented model. Experimental and theoretical spectra show an excellent match.

The thicknesses of our films obtained by Far – infrared spectroscopy are 20% greater, which is within the limits of error for both techniques. When using Far – infrared spectroscopy for calculating thickness of layered structured, we bring errors in absolute measurements, because we calculate effective thickness. The important thing is, the trend is the same, the films does not differ in the relative thickness, i.e. thickness ratios between films are the same.

We note that the thickness (d) of the film changes in the range of ~0.39–~0.7 μm. While the thickness of the film is in the 0.40 μm region, the crystallite size is about 32 nm, and for a film thickness of about 0.72 μm, we have two sizes of crystallites different for a factor of 2. In addition, from Table 1, we have for thicker films CdTe 1 and CdTe 3, that the position of the coupled plasmon-phonon mode ω_{l1} is below the values of $\omega_{LO,CdTe} = 170.5\ cm^{-1}$. On the other hand, these values are above $\omega_{LO,CdTe}$ for thin films CdTe 2 and CdTe 4. In both cases plasmon damping (Γ_p) is relatively low. The obtained eigenfrequencies of the plasmon – phonon coupled modes for CdTe thin films are presented in Fig. 8. As a result of the best fit from Fig. 7, we obtained the frequencies of coupled modes (ω_{l1} and ω_{l2}) marked by open circles and transverse mode frequencies which are denoted by - x. Value of ω_P are calculated by Refs. [16–18]:

$$\omega_P = \frac{\omega_{l1}\omega_{l2}}{\omega_t} \tag{8}$$

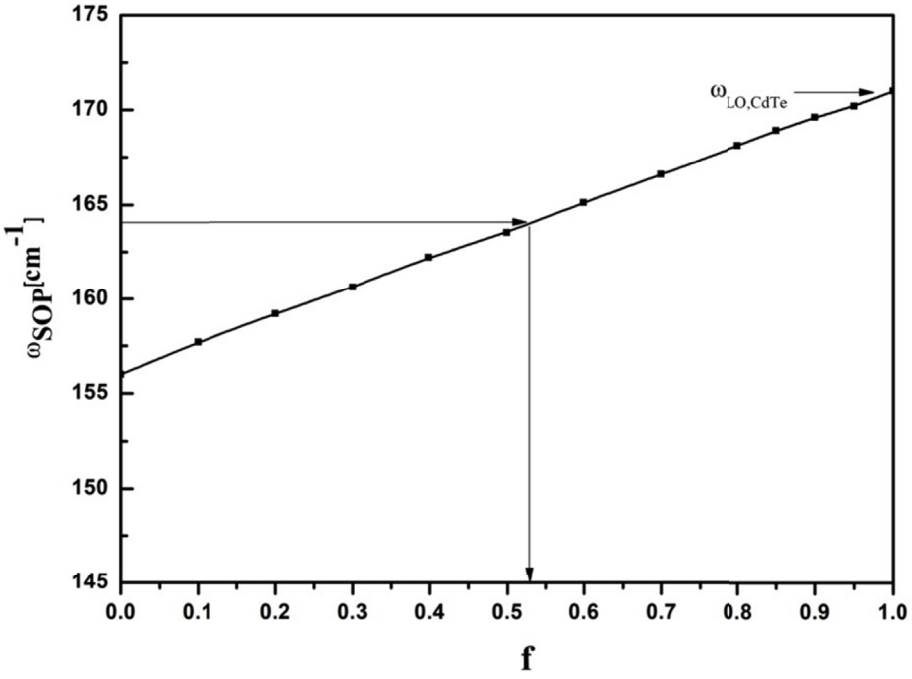

Fig. 5. Surface optical phonon (SOP) mode position vs. filing factor.

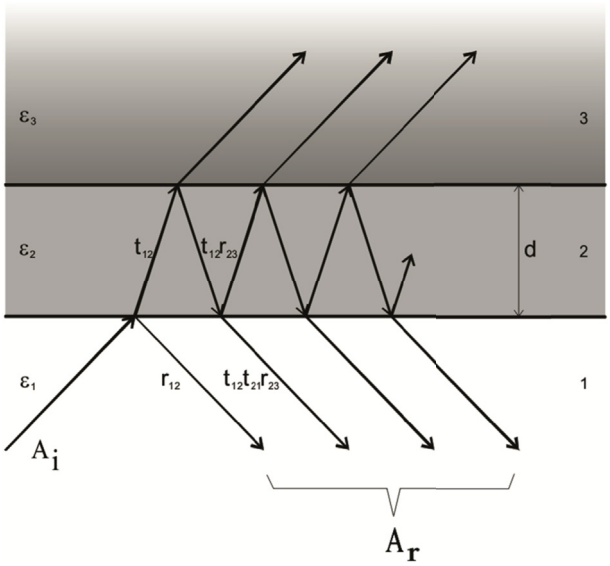

Fig. 6. Schematic presentation of a three layer structure [46].

The calculated lines at Fig. 7 are solution of a real part of uncoupled dielectric function (Eq. (1)). However, for plasma-phonon modes positions are obtained:

$$\omega_{\pm} = \frac{\omega_P^2 + \omega_{LO}^2}{2} \pm \sqrt{\frac{(\omega_P^2 + \omega_{LO}^2)^2 - \omega_P \omega_{TO}}{4}} \quad (9)$$

The full lines in Fig. 7 were obtained for the case $\omega_{LO,CdTe} = 170.5\,cm^{-1}$. It is clear that all values of ω_{l1} and ω_{l2} are out of this theoretical model. Best fit, dashed lines in Fig. 7, was obtained for $\omega_{SOP} = 164\,cm^{-1}$ which in Eq. (9) plays a role ω_{LO}. Shift of about $7\,cm^{-1}$ is registered in relation to $\omega_{LO,CdTe}$, just like in the case of Raman spectra. As we said earlier, the LO phonon shift of CdTe crystal is attributed to the surface optical phonon (SOP) mode effect.

Based on these results, it is clear that in the case of CdTe thin films, prepared by using thermal evaporation technique, the filing factor is constant and does not depend on film thickness, crystallite size and

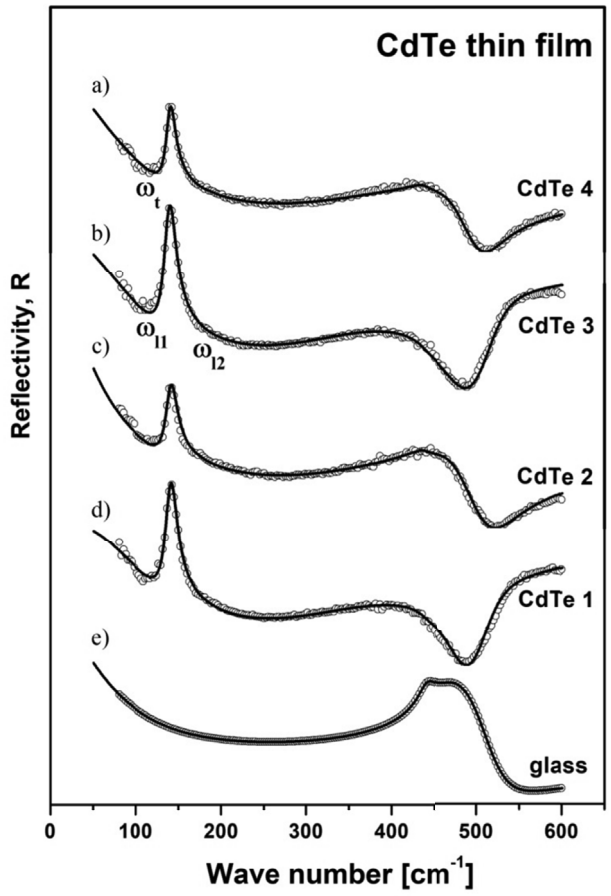

Fig. 7. Far – infrared reflection spectra of: CdTe thin films with thickness of (a) 0.39 μm, (b) 0.71 μm, (c) 0.43 μm, (d) 0.72 μm, and glass substrate (e). Experimental spectra are presented by circles while solid lines are calculated spectra obtained by a fitting procedure based on the model given by Eqs. (2) and (4)–(7).

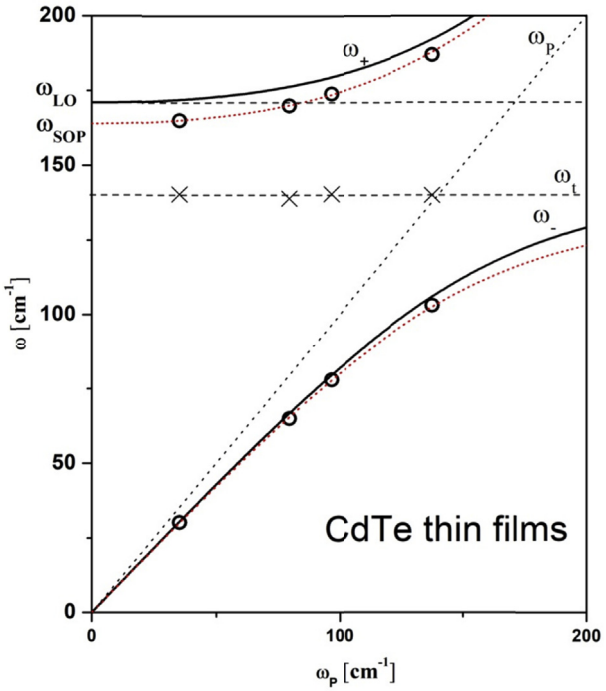

Fig. 8. The eigenfrequencies of the plasmon–phonon modes for CdTe thin films. The lines are calculated spectra [Re{ε_2} = 0; ε_2 is given by Eq. (1)]: solid line with $\omega_{LO,CdTe}$ = 170.5 cm^{-1}; dashed line with ω_{SOP} = 164 cm^{-1}; ○ - ω_{l1}, ω_{l2}; x – ω_t.

concentration of free carriers. On the other hand, the reflection spectra depend on the thickness of the film and the concentration of free carriers in the film, which is expected. In general, thin films have a higher concentration of free carriers ($\sim\omega_p$) (see Table 1). The linear dependence of the position of the SOP mode on the filing factor causes the existence of a modified plasmon – phonon interaction, where the SOP has the role of the LO phonon.

Of course, there are many models that can describe the registered frequency shift of the LO phonon in CdTe e.g. a continuum model of the optical phonon confinement [47,48] would also give a shift of 7 cm^{-1}, but for spherical nanoparticles of about 5 nm, which is far from our case.

4. Conclusion

In this paper, we present results of investigation of CdTe thin films prepared with thermal evaporation technique, with different thicknesses. Sample's surfaces are rather flat, but still they are characterized with bright protrusions and dark holes (air) resulting in a small surface roughness of several nanometers. We showed that, when using thermal evaporation technique we get high quality thin films, especially for thicker films with greater crystallite size. We conclude that the filling factor of our thin films is constant and does not depend on film thickness, crystallite size or concentration of free carriers, but yet has linear dependence on SOP position. This kind of morphology, with filling factor of ~50% causes existence of surface optical phonon and its interaction with plasmon, because of the free surface around nanoparticles. A numerical model for calculating the reflectivity coefficient for complex system, which includes films and substrate, has been applied, and CdTe thin film were treated as a mixture of homogenous spherical inclusion in air modeled by Maxwell – Garnet formula.

Acknowledgements

This research was financially supported by the Serbian Ministry of Education and Science (Project 45003) and in Poland by National Science Center granted under decision No. DEC-2011/01/B/ST5/06602. The authors would like to express their gratitude to King Khalid University, Saudi Arabia for providing administrative and technical support.

References

[1] S. Chandra Ray, K. Mallick, Int. J. Chem. Eng. Appl. 4 (2013) 183–186.
[2] C.S. Ferekides, U. Balasubramanian, R. Mamazza, V. Viswanathan, H. Zhao, D.L. Morel, Sol. Energy 77 (2004) 823–830.
[3] R. Kulkarni, et al., Energy Procedia 110 (2017) 188–195.
[4] A. Arnoult, J. Cibert, Appl. Phys. Lett. 66 (1995) 2397–2399.
[5] P. Bhattacharya, D.N. Bose, Semicond. Sci. Technol. 6 (1991) 384–387.
[6] A.U. Ubale, D.K. Kulkarni, Indian J. Pure Appl. Phys. 44 (2006) 254–259.
[7] T.L. Chu, S.S. Chu, C. Ferekides, J. Britt, C.Q. Wu, J. Appl. Phys. 71 (1992) 3870.
[8] A. Nakano, et al., Sol. Cell. 17 (1986) 233.
[9] K.S. Rahman, F. Haque, 3rd International Conference on the Developments in Renewable Energy Technology (ICDRET), 2014, pp. 29–31.
[10] S. Lalitha, S. Zh Karazhanov, P. Ravindran, S. Senthilarasu, R. Sathyamoorthy, J. Janabergenov, Physica B 387 (2007) 227–238.
[11] S. Singh, et al., Thin Solid Films 519 (2010) 1078–1081.
[12] D.S. Chuu, C.M. Dai, W.F. Hsieh, C.T. Tsai, J. Appl. Phys. 69 (1991) 12.
[13] A. Singha, B. Satpati, P.V. Satyam, A. Roy, J. Phys. Condens. Mater. 17 (2005) 5708–5967.
[14] M. Gilić, J. Trajić, N. Romčević, M. Romčević, D.V. Timotijević, G. Stanišić, I.S. Yahia, Opt. Mater. 35 (2013) 1112–1117.
[15] M. Cardona (Ed.), Top. Appl. Phys, vol. 8, Springer, Berlin, 1975.
[16] N. Romčević, M. Romčević, A. Golubović, Le Van Khoi, A. Mycielski, Đ. Jovanović, D. Stojanović, S. Nikolić, S. Đurić, J. Alloy. Compd. 397 (2005) 52–57.
[17] M. Romčević, N. Romčević, V.N. Nikiforov, Infrared Phys. Technol. 42 (2001) 541–545.
[18] N. Romčević, M. Romčević, A. Milutinović, S. Kostić, J. Alloy. Compd. 478 (2009) 41–44.
[19] J. Trajić, M. Romčević, N. Romčević, B. Babić, B. Matović, P. Balaž, Opt. Mater. 57 (2016) 225–230.
[20] N. Romčević, M. Romčević, W.D. Dobrowolski, L. Kilanski, M. Petrović, J. Trajić, B. Hadzić, Z. Lazarević, M. Gilić, J.L. Ristic-Djurović, N. Paunović, A. Reszka, B.J. Kowalski, I.V. Fedorchenko, S.F. Marenkin, J. Alloy. Compd. 649 (2015) 375–379.
[21] J. Trajić, N. Romčević, M. Romčević, V.N. Nikiforov, Mater. Res. Bull. 42 (2007) 2192–2201.
[22] M. Romčević, N. Romčević, W. Dobrowolski, L. Kalinski, J. Trajić, D.V. Timotijević, E. Dynowska, I.V. Fedorchenko, S.F. Marenkin, J. Alloy. Compd. 548 (2013) 33–37.
[23] N. Romčević, J. Trajić, T.A. Kuznetsova, M. Romčević, B. Hadžić, D.R. Khokhlov, J. Alloy. Compd. 442 (2007) 324–327.
[24] J. Trajić, N. Romčević, M. Romčević, D. Stojanović, R. Rudolf, T.A. Kuznetsova, D.R. Khokhlov, J. Alloy. Compd. 493 (2010) 41–46.
[25] J. Trajić, N. Romčević, M. Romčević, D. Stojanović, L.I. Ryabova, D.R. Khokhlov, J. Alloy. Compd. 602 (2014) 300–305.
[26] R.W. Cheary, A. Coelho, J. Appl. Crystallogr. 25 (1992) 109–121.
[27] R. Triboulet & P. Siffert, first ed., Elsevier, 2010.
[28] H. Zeng, W. Cai, B. Cao, J. Hu, Y. Li, P.S. Liu, Appl. Phys. Lett. 88 (2006) 181905.
[29] A. Ghosh, R.N.P. Chodhary, J. Phys. D Appl. Phys. 42 (2009) 075416.
[30] F. Friedrich, N.H. Nickel, Appl. Phys. Lett. 91 (2007) 111903.
[31] J. Xu, W. Ji, X.B. Wang, H. Shu, Z.X. Shen, S.H. Tang, J. Raman Spectrosc. 29 (1998) 613.
[32] V.C. Stergiou, Y.S. Raptis, E. Anastassakis, N. Pelekaneos, A. Nahmani, J. Cibert, Phys. Status Solidi 223 (2001) 237.
[33] J.F. Scott, T.C. Damem, Optic Commun. 5 (1972) 410.
[34] R. Rossetti, S. Nakahara, L.E. Bru, J. Chem. Phys. 79 (1983) 1086.
[35] B.F. Variano, N.E. Schlotter, D.M. Hwangand, C.J. Sandroff, J. Chem. Phys. 88 (1988) 2848.
[36] A.V. Baranov, Y.S. Bobovich, N.I. Grebenshchikova, V.I. Petrov, M.Y. Tsenter, Optic Spectrosc. 60 (1986) 685.
[37] H. Jerominek, M. Pigeon, S. Patela, Z. Jakubczk, C. Delisle, R.J. Tremblay, Appl. Phys. 63 (1986) 957.
[38] E.F. Hilinski, P.A. Lucas, J. Chem. Phys. 89 (1988) 3435.
[39] J. Trajić, M. Gilić, N. Romčević, M. Romčević, G. Stanišić, B. Hadžić, M. Petrović, Y.S. Yahia, Sci. Sinter. 47 (2015) 145–152.
[40] G. Irmer, J. Raman Spectrosc. 38 (2007) 634.
[41] K. Karkkainen, A. Saviola, K. Nikoskinen, IEEE Trans. Geosci. Rem. Sens. 39 (5) (2001) 1013.
[42] J.C.M. Garnett, Trans. Roy. Soc. Can. CIII (1904) 385420.
[43] A. Saviola, I. Lindell, A. Priou (Ed.), Dielectric Properties of Heterogeneous Materials PIER 6 Progres in Electromagnetic Research, Elsevier, Amsterdam, 1992, pp. 101–115 1.
[44] B. Hadzić, N. Romcević, M. Romcević, I. Kuryliszyn-Kudelska, W. Dobrowolski, J. Trajić, D.V. Timotijević, U. Narkiewicz, D. Sibera, J. Alloy. Compd. 540 (2012) 49–56.
[45] M. Gilić, et al., Infrared Phys. Technol. 76 (2016) 276–284.
[46] J. Trajić, M. Gilić, N. Romčević, M. Romčević, G. Stanišić, Z. Lazarević, D. Joksimović, I.S. Yahia, Phys. Scr., T 162 (2014) 014031.
[47] R. Roca, C. Trallero-Giner, M. Cardona, Phys. Rev. B 49 (1994) 13704.
[48] M.P. Chamberlain, C. Trallero-Giner, M. Cardona, Phys. Rev. B 51 (1995) 1680.